IEEE Access
Multidisciplinary | Rapid Review | Open Access Journal

Received 10 November 2022, accepted 5 December 2022, date of publication 23 December 2022, date of current version 2 January 2023.

Digital Object Identifier 10.1109/ACCESS.2022.3231895

RESEARCH ARTICLE

A Novel Ergodic Cellular Automaton Model of Gene-Protein Network: Theoretical Nonlinear Analyses and Efficient FPGA Implementation

SHOGO SHIRAFUJI, (Student Member, IEEE), AND HIROYUKI TORIKAI, (Member, IEEE)
Graduate School of Science and Engineering, Hosei University, Koganei-shi, Tokyo 184-8584, Japan

Corresponding author: Shogo Shirafuji (s.shirafuji@ieee.org)

This work was supported in part by JSPS KAKENHI under Grant 21H03515, and in part by the Support Center for Advanced Telecommunications Technology Research in Japan.

ABSTRACT A novel ergodic cellular automaton model of gene-protein network is presented. It is shown that the presented model can predict occurrences of typical nonlinear phenomena of a conventional ordinary differential equation gene-protein network model. In addition, theoretical analysis methods of the presented model are proposed. Using the analysis methods, an important advantage of the presented model is revealed: the ergodic cellular automaton is better suited to predict the occurrences of the nonlinear phenomena of the differential equation gene-protein network model compared to a regular (standard) cellular automaton. Furthermore, the presented model is implemented by a field programmable gate array and experiments validate its operations. It is then revealed that the presented model is much more hardware-efficient compared to a standard numerical integration formula of the differential equation model.

INDEX TERMS Gene-protein network, cellular automaton, nonlinear dynamics bifurcation phenomena, field programmable gate array.

I. INTRODUCTION

A wide variety of gene-protein network [1], [2], [3] simulators [4] have been developed with emphasis on their applications in drug discovery for personalized medicine [5], where most of them have been implemented as softwares executed on general purpose digital processors. To apply a gene-protein network simulator for personalized medicine, it is important to fit parameter values of the network model so that it reproduces behaviors of a biological gene-protein network of an objective patient. Recently, metaheuristics (e.g., particle swarm optimization and genetic algorithm) have been successfully utilized to fit parameter values of gene-protein network models [6]. The problems in the metaheuristics of the gene-protein network model include requirement of (a) *long computational time* and (b) *large electric energy* to operate the network model for a large number of different parameter values. Since the operations of the network model in the metaheuristics are basically independent, they can be executed simultaneously by using multiple network models. Therefore, parallel operations of multiple network models can accelerate the computational time of the parameter fitting. Hence, in order to overcome the problems in the parameter fitting of the gene-protein network model for personalized medicine (e.g., the requirements of (a) long computational time and (b) large electric energy), it is important to design a network model that consumes few circuit elements and low energy to realize efficient parallel operations. Then the goal of this study is set to design an application special electronic circuit model, which is especially designed to reproduce behaviors of a gene-protein network and consumes fewer circuit elements and lower energy compared to conventional gene-protein network models. To realize such a hardware-efficient gene-protein network model, in this study, the concept of *ergodic cellular automaton biomimetic circuit* [7] is employed, where its relations to other biomimetic circuits are summarized as follows. The biomimetic circuits can be classified into the following four classes based on

The associate editor coordinating the review of this manuscript and approving it for publication was Ludovico Minati.

their fundamental properties (i.e., continuousness of time and state-space) of mathematical modeling methods.

1) CLASS CTCS BIOMIMETIC CIRCUIT

A nonlinear differential equation model of a biomimetic circuit has a *continuous* time and a *continuous* state-space and is implemented by a nonlinear dynamic circuit typically.

2) CLASS DTCS BIOMIMETIC CIRCUIT

A nonlinear difference equation model of a biomimetic circuit has a *discrete* time and a *continuous* state-space and is implemented by a nonlinear switched capacitor circuit typically.

3) CLASS DTDS BIOMIMETIC CIRCUIT

A digitally implemented numerical integration model of a biomimetic circuit has a *discrete* time and a *discrete* state-space and is implemented by a digital processor typically. In addition, a regular (standard) cellular automaton model of a biomimetic circuit also belongs to the class DTDS circuit and is implemented by a synchronous sequential logic typically.

4) CLASS CTDS BIOMIMETIC CIRCUIT

An asynchronous cellular automaton model of a biomimetic circuit has a *continuous* state transition time and a *discrete* state-space, and is implemented by an asynchronous sequential logic typically.

Most biomimetic circuits belong to the class CTCS, DTCS, and DTDS circuits [9], [10], [11], [12]. On the contrary, our group has developed several kinds of asynchronous cellular automaton biomimetic circuits (e.g., central pattern generator model, neural network model, neuron model, and cochlea model [13], [14], [15], [16]), which belong to the class CTDS circuit. In addition, very recently, our group has just proposed the concept of *ergodic cellular automaton biomimetic circuit* [7], which can be regarded as a generalization of the asynchronous cellular automaton biomimetic circuit and is more suitable for implementation. The advantages of the ergodic cellular automaton biomimetic circuits include capabilities of implementation by fewer circuit elements and operation with lower energy consumption compared to digital processor biomimetic circuits.

Based on the above-mentioned backgrounds on the importance of the gene-protein network model and the advantages of the ergodic cellular automaton biomimetic circuit, in this paper, a novel ergodic cellular automaton gene-protein network is presented, and its advantages are revealed as follows. In Section II, a typical conventional nonlinear ordinary differential equation (ODE) model of gene-protein network is introduced. It is explained that the ODE gene-protein network model exhibits several nonlinear phenomena. In Section III, inspired by the nonlinear vector field of the ODE, the novel ergodic cellular automaton model of the gene-protein network is presented. It is shown that the presented model can predict occurrences of typical nonlinear phenomena of the ODE model. In Section IV, theoretical analysis methods of the ergodic cellular automaton gene-protein network model

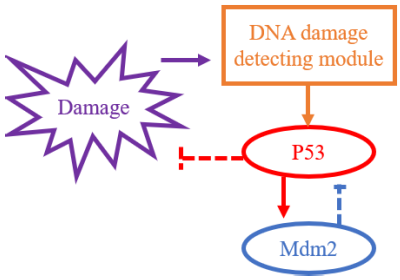

FIGURE 1. Schematic diagram of a gene-protein network model [18].

are proposed. Using the analysis methods, it is revealed that the ergodic cellular automaton is better suited to model the gene-protein network compared to a regular (standard) cellular automaton. In Section V, the presented model is implemented by a field programmable gate array (FPGA) and experiments validate its operations. It is revealed that the presented ergodic cellular automaton gene-protein network can be implemented by much fewer circuit elements and consumes much lower energy compared to a standard numerical integration formula of the ODE gene-protein network model. The novelty and the significance of this study include the following points.

A. NOVELTY

The presented model is the first gene-protein network model that is designed based on the concept of the ergodic cellular automaton biomimetic circuit.

B. SIGNIFICANCE

The analysis results of this study reveal that the ergodic cellular automaton is suited to model the gene-protein network. In addition, the comparison results of this study reveal that the presented ergodic cellular automaton gene-protein network model is hardware-efficient. Hence these results will provide fundamental knowledge about designing a hardware-efficient application specific integrated circuit for the genome simulation.

II. AN ODE GENE-PROTEIN NETWORK MODEL

As a preparation to design a novel hardware-efficient gene-protein network model in the next section, an ordinary differential equation (ODE) gene-protein network model describing a DNA damage repair function [17] is introduced in this section. Fig. 1 shows the structure of the network model. The model has the following state variables.

$$\begin{aligned} x \in \boldsymbol{R}^{+} &\text{corresponding to concentration of} \\ &\text{protein 53 (p53),} \\ y \in \boldsymbol{R}^{+} &\text{corresponding to concentration of} \\ &\text{murine double minute 2 (Mdm2),} \end{aligned}$$

where $\boldsymbol{R}^{+} = \{r | r \in \boldsymbol{R},\ r \geq 0\}$. The dynamics of the network model is described by the following ODE.

$$\frac{dx}{dt} = \alpha_0 + \frac{\alpha_1 x^n}{k_1 + x^n} - \gamma_1 xy - \gamma_2 x,$$

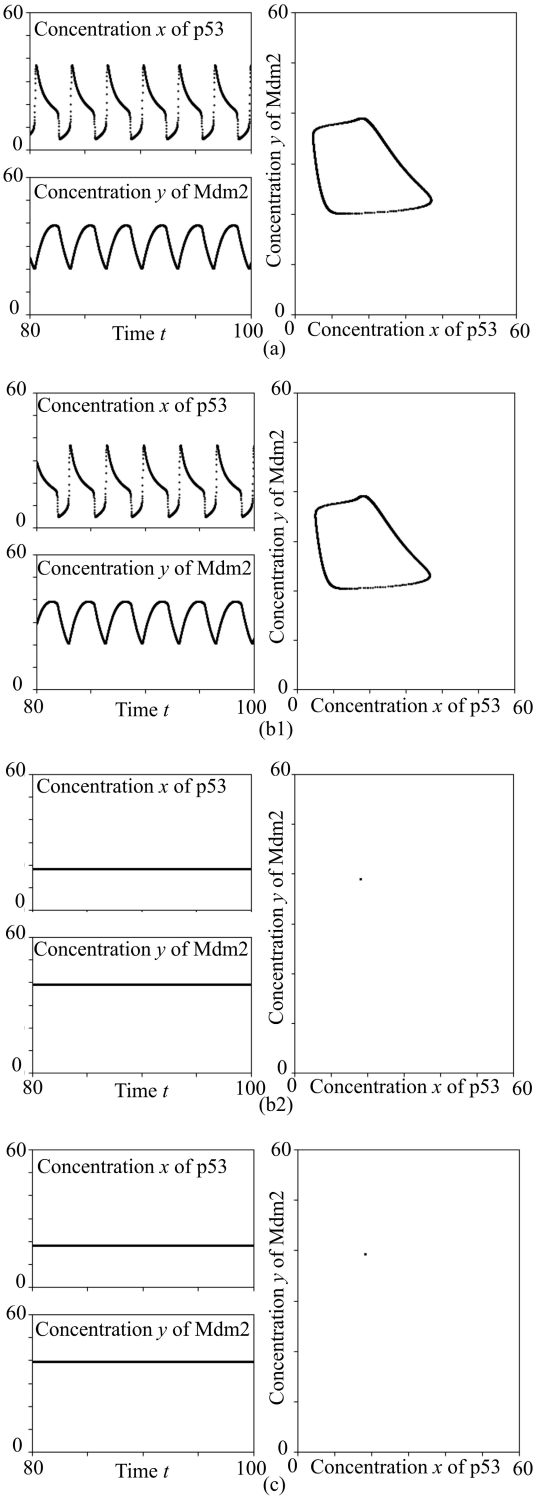

FIGURE 2. Typical time waveforms and corresponding phase plane trajectories of the gene-protein network model in Eq. (1). $(n, \alpha_1, \alpha_2, \alpha_3, k_1, k_2, \gamma_1, \gamma_2, \gamma_3) = (6, 700, 0.05, 40, 10000000, 50000, 1, 1, 0.7)$ [19]. (a) Stable periodic orbit. $\alpha_0 = 175$. (b) Co-existence of stable periodic orbit in (b1) and stable equilibrium point in (b2). $\alpha_0 = 179.4$. (c) Stable equilibrium point. $\alpha_0 = 185$.

$$\frac{dy}{dt} = \alpha_2 + \frac{\alpha_3 x^4}{k_2 + x^4} - \gamma_3\, y. \tag{1}$$

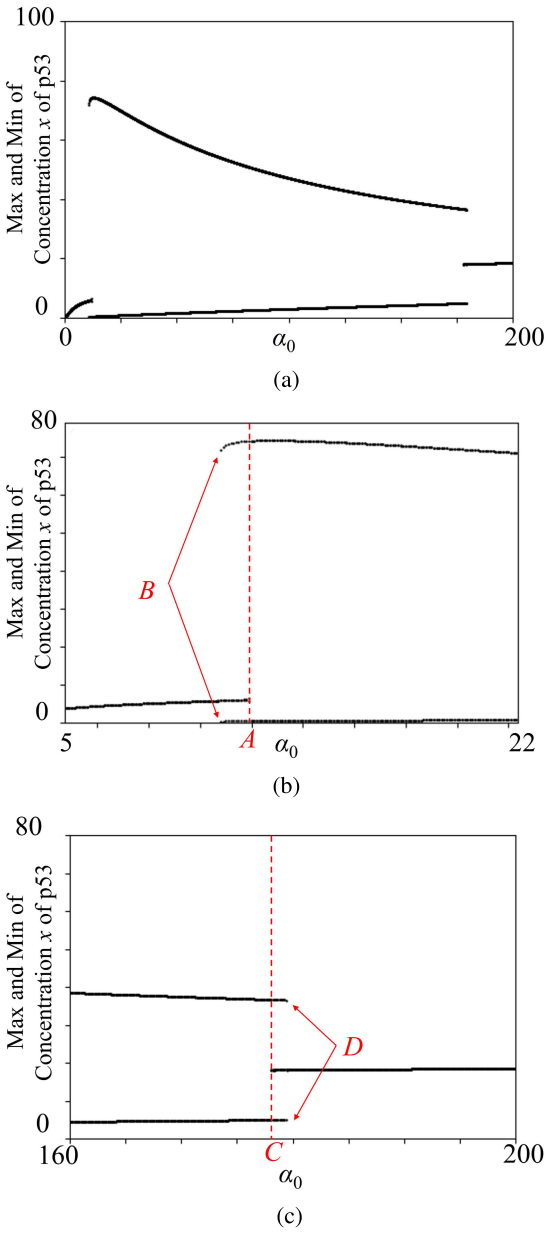

FIGURE 3. (a) Characteristics of the ODE gene-protein network model in Eq. (1). The horizontal axis is the reproduction rate α_0 of p53. The vertical axis is the maximum and the minimum values of the p53 concentration x in a steady state. (b) Enlargement of the graph in (a) near $\alpha_0 = 10$. The model exhibits a subcritical Andronov-Hopf bifurcation at *A* and a fold limit cycle bifurcation at *B*. (c) Enlargement of the graph in (a) near $\alpha_0 = 180$. The model exhibits a subcritical Andronov-Hopf bifurcation at *C* and a fold limit cycle bifurcation at *D*.

Fig. 2 depicts typical time waveforms and corresponding phase plane trajectories of the network model. As shown in the figure, the model exhibits the following nonlinear phenomena.

A. STABLE PERIODIC ORBIT

In the case of Fig. 2(a), the network exhibits a stable periodic orbit. In the context of the DNA damage repair function, the periodic oscillation of the p53 concentration x means that the network is trying to repair DNA damage repeatedly.

B. STABLE EQUILIBRIUM POINT

In the case of Fig. 2(c), the network exhibits a stable equilibrium point. In the context of the DNA damage repair function, the stable equilibrium point means that the repair function of the network is not activated.

C. CO-EXISTENCE

In the case of Figs. 2(b1) and (b2), the network exhibits co-existence of a stable periodic orbit in (b1) and a stable equilibrium point in (b2), i.e., the network exhibits either (b1) or (b2) depending on the initial condition.

Fig. 3 depicts the characteristics of the p53 concentration x for the parameter α_0, which corresponds to the reproduction rate of the p53. It can be confirmed that the network model exhibits the following nonlinear phenomena.

D. SUBCRITICAL Andronov-Hopf BIFURCATION

At the point A in Fig. 3(b), the stable equilibrium point (which inactivates the DNA damage repair function) changes to the stable periodic orbit (which activates the DNA damage repair function) as the reproduction rate α_0 of p53 increases. This change of phenomena is caused by a subcritical Andronov-Hopf bifurcation [20]. Note that the network model has co-existing stable equilibrium point and stable periodic orbit between the points A and B.

E. SUBCRITICAL Andronov-Hopf BIFURCATION (OPPOSITE DIRECTION)

At the point C in Fig. 3(c), the stable equilibrium point (which inactivates the DNA damage repair function) changes to the stable periodic orbit (which activates the DNA damage repair function) as the reproduction rate α_0 of p53 decreases. This change of phenomena is also caused by a subcritical Andronov-Hopf bifurcation. Note that the network model has co-existing stable equilibrium point and stable periodic orbit between the points C and D.

F. FOLD LIMIT CYCLE BIFURCATION

At the point B in Fig. 3(b), the stable periodic orbit disappears as the reproduction rate α_0 of p53 decreases. This change of phenomena is caused by a fold limit cycle bifurcation [20]. At the point D in Fig. 3(c), the stable periodic orbit disappears as the reproduction rate α_0 of p53 increases. This change of phenomena is also caused by a fold limit cycle bifurcation.

In the next section, a novel ergodic cellular automaton gene-protein network model that can reproduce the above nonlinear phenomena is presented.

III. NOVEL ERGODIC CELLULAR AUTOMATON GENE-PROTEIN NETWORK MODEL

A. MODEL DESCRIPTION

In this section, the novel hardware-efficient model of the gene-protein network is presented. Fig. 4 shows a schematic circuit diagram of the presented model. The model has two

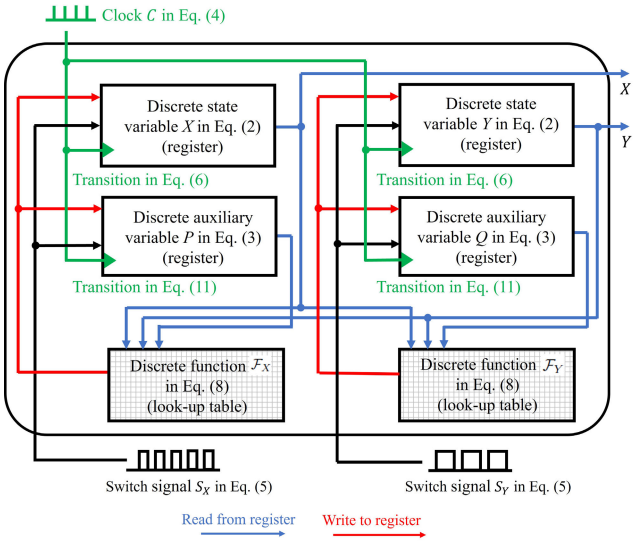

FIGURE 4. Schematic circuit diagram of the presented gene-protein network model.

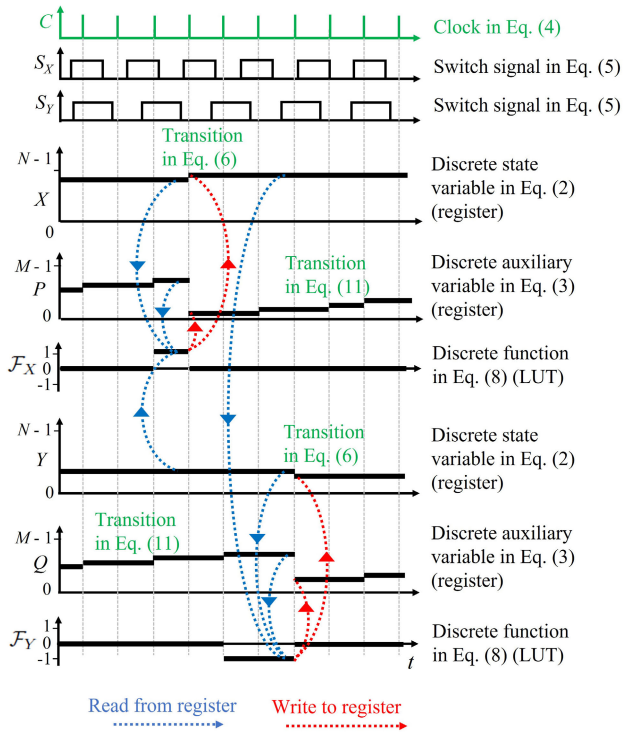

FIGURE 5. Timing chart of the presented gene-protein network model.

registers storing the following discrete state variables.

$$X \in \boldsymbol{Z}_N \quad \text{corresponding to concentration } x \text{ of p53},$$
$$Y \in \boldsymbol{Z}_N \quad \text{corresponding to concentration } y \text{ of Mdm2},$$
$$\boldsymbol{Z}_N = \{0, 1, \cdots, N-1\}, \tag{2}$$

where the variables are saturated at 0 and $N-1$. The presented model also has two registers storing the following discrete auxiliary variables.

$$P \in \boldsymbol{Z}_M \quad \text{adjusting velocity of } X,$$

$$Q \in \mathbf{Z}_M \quad \text{adjusting velocity of } Y,$$
$$\mathbf{Z}_M = \{0, 1, \cdots, M-1\}, \tag{3}$$

where the variables are saturated at 0 and $M-1$. As shown in Fig. 4, the presented model receives the following periodic clock $C(t)$ (see also timing chart in Fig. 5).

$$C(t) = \sum_{n=0}^{\infty} p(t - nT), \quad p(t) = \begin{cases} 1 \text{ if } t = 0, \\ 0 \text{ if } t \neq 0, \end{cases} \tag{4}$$

where $T > 0$ is a period of the clock $C(t)$ and $p(t)$ is an instantaneous pulse corresponding to a positive edge of a rectangular-shaped clock signal. In addition, the presented model receives the following two periodic binary signals $S_X(t)$ and $S_Y(t)$ (see also timing chart in Fig. 5).

$$S_X(t) = \sum_{n=0}^{\infty} q(t - nT_X - \Phi_X, W_X),$$
$$S_Y(t) = \sum_{n=0}^{\infty} q(t - nT_Y - \Phi_Y, W_Y),$$
$$q(t, W) = \begin{cases} 1 \text{ if } t \in [0, W], \\ 0 \text{ if } t \notin [0, W], \end{cases} \tag{5}$$

where $T_X > 0$ and $T_Y > 0$ are periods, $W_X \in [0, T_X]$ and $W_Y \in [0, T_Y]$ are pulse durations, and $\Phi_X \in [0, T_X)$ and $\Phi_Y \in [0, T_Y)$ are initial phases of the binary signals $S_X(t)$ and $S_Y(t)$, respectively. Then the clock $C(t)$ induces the following transitions of the discrete state variables X and Y (see also timing chart in Fig. 5).

1) TRANSITIONS OF STATE VARIABLES

$$\begin{aligned} &\text{If } C(t) = 1, \text{ then} \\ &X(t^+) = X(t) + S_X(t)\mathcal{F}_X(X(t), Y(t), P(t)), \\ &Y(t^+) = Y(t) + S_Y(t)\mathcal{F}_Y(X(t), Y(t), Q(t)), \end{aligned} \tag{6}$$

where $t^+ = \lim_{\epsilon \to 0} + \epsilon$ and $\epsilon > 0$, and the discrete functions

$$\mathcal{F}_X : \mathbf{Z}_N^2 \times \mathbf{Z}_M \to \{-1, 0, 1\},$$
$$\mathcal{F}_Y : \mathbf{Z}_N^2 \times \mathbf{Z}_M \to \{-1, 0, 1\}, \tag{7}$$

determine the nonlinear vector field of the presented model. To reproduce the nonlinear vector field of the ODE gene-protein network model in Eq. (1), we propose to design the discrete functions $\mathcal{F}_X$ and $\mathcal{F}_Y$ as follows.

$$\mathcal{F}_X(X, Y, P) = \begin{cases} 1 & \text{if } F_X(X, Y) \geq 0 \text{ and } P \geq |F_X(X, Y)|, \\ -1 & \text{if } F_X(X, Y) < 0 \text{ and } P \geq |F_X(X, Y)|, \\ 0 & \text{otherwise,} \end{cases}$$
$$\mathcal{F}_Y(X, Y, Q) = \begin{cases} 1 & \text{if } F_Y(X, Y) \geq 0 \text{ and } Q \geq |F_Y(X, Y)|, \\ -1 & \text{if } F_Y(X, Y) < 0 \text{ and } Q \geq |F_Y(X, Y)|, \\ 0 & \text{otherwise,} \end{cases} \tag{8}$$

where the functions F_X and F_Y are defined by

$$F_X(X, Y) = Int(f_X(X, Y)^{-1} T_X^{-1}),$$
$$F_Y(X, Y) = Int(f_Y(X, Y)^{-1} T_Y^{-1}),$$
$$F_X : \mathbf{Z}_N^2 \to \mathbf{Z}_M^{\pm}, \quad F_Y : \mathbf{Z}_N^2 \to \mathbf{Z}_M^{\pm},$$
$$\mathbf{Z}_M^{\pm} = \{-(M-1), -(M-2), \cdots, M-1\}, \tag{9}$$

which are saturated at $-(M-1)$ and $M-1$, and the function $Int(x)$ gives the integer part of x. The functions f_X and f_Y used in F_X and F_Y are defined by

$$f_X(X, Y) = \Omega_X \left(\alpha_0 + \frac{\alpha_1 (\frac{X}{\Omega_X})^n}{(k_1 + (\frac{X}{\Omega_X})^n)} - \gamma_1 \frac{X}{\Omega_X} \frac{Y}{\Omega_Y} - \gamma_2 \frac{X}{\Omega_X} \right),$$
$$f_Y(X, Y) = \Omega_Y \left(\alpha_2 + \frac{\alpha_3 (\frac{X}{\Omega_X})^4}{(k_2 + (\frac{X}{\Omega_X})^4)} - \gamma_3 \frac{Y}{\Omega_Y} \right), \tag{10}$$

where Ω_X and Ω_Y are scaling parameters. Then the clock $C(t)$ induces the following transitions of the discrete auxiliary variables P and Q (see also timing chart in Fig. 5).

2) TRANSITIONS OF AUXILIARY VARIABLES

$$\begin{aligned} &\text{If } C(t) = 1 \text{ and } S_X(t) = 1, \text{ then} \\ &P(t^+) = \begin{cases} P(t) + 1 & \text{if } \mathcal{F}_X(X(t), Y(t), P(t)) = 0, \\ 0 & \text{otherwise,} \end{cases} \\ &\text{If } C(t) = 1 \text{ and } S_Y(t) = 1, \text{ then} \\ &Q(t^+) = \begin{cases} Q(t) + 1 & \text{if } \mathcal{F}_Y(X(t), Y(t), Q(t)) = 0, \\ 0 & \text{otherwise.} \end{cases} \end{aligned} \tag{11}$$

B. MATHEMATICAL OPERATIONS AND HARDWARE

In the circuit schematic in Fig. 4 and the timing chart in Fig. 5, relations between the mathematical operations and the hardware are illustrated as follows.

- The discrete variables (X, Y, P, Q) defined in Eqs. (2) and (3) are stored in the registers.
- The discrete functions $(\mathcal{F}_X, \mathcal{F}_Y)$ defined in Eq. (8) are implemented as look-up tables (LUTs).
- The transitions in Eqs. (6) and (11) of the discrete variables (X, Y, P, Q) are triggered by the clock C and are realized by updating the values of the registers.

In Fig. 5, timings of memory accesses (i.e., reads from registers and writes to registers) are illustrated. It can be confirmed that, since the values stored in the four registers can be updated simultaneously at the same clock timing, the possible maximum number of state transitions that can be executed simultaneously is four, which can be regarded as a degree of parallelism (i.e., a degree of parallel operations of the transitions in Eqs. (6) and (11)) of the presented model.

Note that the ODE gene-protein network model in Eq. (1) has the autonomous nonlinear dynamics and no input. Since the presented model is designed to mimic the autonomous model in Eq. (1), from a viewpoint of the dynamical system theory, the presented model can be regarded to have no input. However, from a viewpoint of the hardware, the

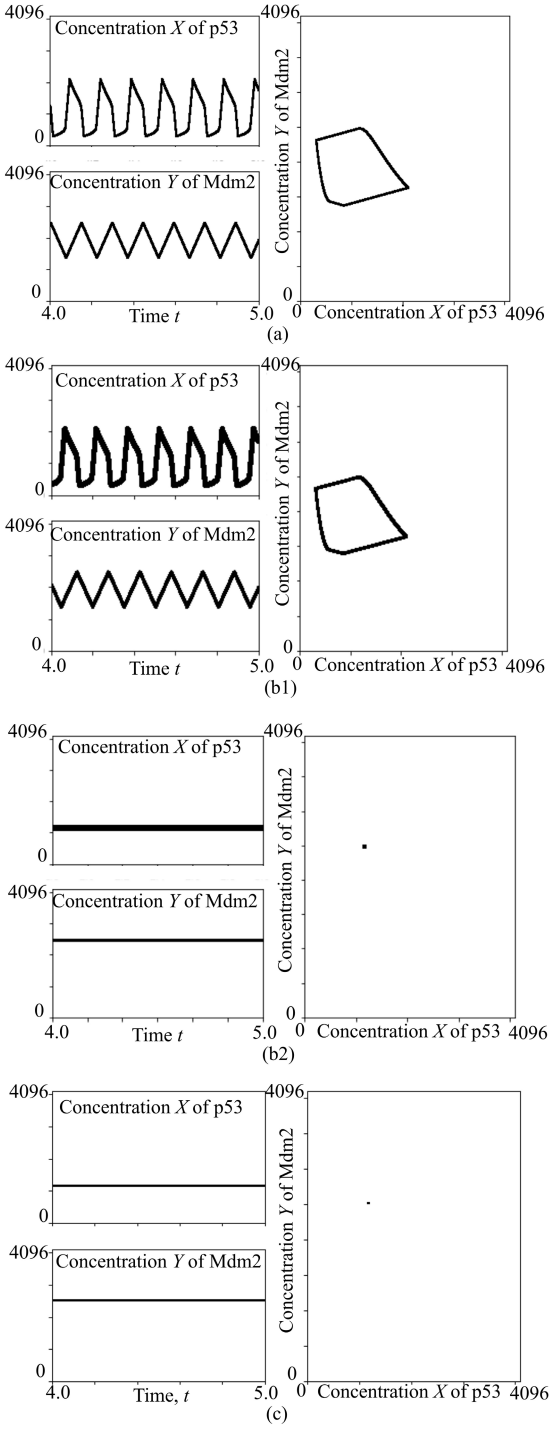

FIGURE 6. Numerical simulations showing typical time waveforms and corresponding phase plane trajectories of the presented gene-protein network model described by Eqs. (6) and (11). $(n, \alpha_1, \alpha_2, \alpha_3, k_1, k_2, \gamma_1, \gamma_2, \gamma_3)$ are as in Fig. 2. $(N, M, T_C, T_X, \Phi_X, W_X, T_Y, \Phi_Y, W_Y, \Omega_X, \Omega_Y) = (4096, 2, 3\sqrt{5}\,10^{-6}, 3\sqrt{5}\,10^{-6}, 0, 3\sqrt{5}\,10^{-6}, 5\sqrt{48}\,10^{-6}, 0, 3\sqrt{5}\,10^{-6}, 64, 64)$. (a) Periodic orbital set O_P. $\alpha_0 = 175$. (b) Co-existence of periodic orbital set O_P in (b1) and stable equilibrium set E in (b2). $\alpha_0 = 179.6$. (c) Stable equilibrium set E. $\alpha_0 = 185$.

presented model accepts the clock C and the switch signals (S_X, S_Y), which can be regarded as inputs to the presented model. In addition, since the discrete state variables (X, Y) are observed for analyses, they can be regarded as outputs of the presented model. Due to the parallelism, the data accesses (i.e., inputs of (S_X, S_Y) and observations of (X, Y) from the outside of the presented model) and the computations (i.e., transitions of the variables (X, Y, P, Q)) are executed at the same clock timing.

C. NUMERICAL SIMULATIONS AND CONTRIBUTIONS

Figs. 6(a), (b), and (c) depict time waveforms and corresponding phase plane trajectories of the presented model obtained by numerical simulations. By comparing with Figs. 2(a), (b), and (c), it can be suggested that the presented model can reproduce the nonlinear phenomena (stable periodic orbit in (a), stable equilibrium point in (b), and coexistence of stable periodic orbit and stable equilibrium point in (c)) of the ODE gene-protein network model in Eq. (1). Fig. 7 depicts the characteristics of the state variable X of the presented model for the parameter α_0. By comparing with Fig. 3, it can be suggested that the presented model can reproduce the nonlinear phenomena (i.e., supercritical Andronov-Hopf bifurcation at A, fold limit cycle bifurcation at B, subcritical Andronov-Hopf bifurcation at C, and fold limit cycle bifurcation at D) of the ODE gene-protein network model. The subsequent sections provide the following contributions.

- In Section IV, theoretical analysis methods of the presented model are provided and the bifurcation phenomena are analyzed theoretically. They are significant to guarantee that the presented model can truly reproduce the bifurcation phenomena of the ODE gene-protein network model.
- In Section V, the presented model is implemented as hardware and comparisons with other implementation methods, including a state-of-the-art soft CPU, are provided. They are significant to show that the presented model is the model of choice for hardware-based gene-protein network simulation.

IV. THEORETICAL ANALYSES

To analyze the nonlinear dynamics of the presented ergodic cellular automaton gene-protein network model, the following state space is defined.

$$\boldsymbol{S} = \{(X, Y) | X \in \boldsymbol{Z}_N, Y \in \boldsymbol{Z}_N\}.$$

Then the following definition for the phenomenon observed in Fig. 6(a) is given.

Definition 1 (Periodic Orbital Set): Suppose there exists a subset $\boldsymbol{O}_p$ of the state space $\boldsymbol{S}$, which satisfies the following three conditions. (a) The subset $\boldsymbol{O}_p$ consists of connected points in the state space $\boldsymbol{S}$, where a point $(X, Y) \in \boldsymbol{S}$ is said to be connected with its eight neighbor points $(X+1, Y)$, $(X+1, Y+1)$, $(X, Y+1)$, $(X-1, Y+1)$, $(X-1, Y)$, $(X-1, Y-1)$, $(X, Y-1)$, and $(X+1, Y-1)$ for $1 \leq X \leq N-2$ and $1 \leq Y \leq N-2$. (b) The subset $\boldsymbol{O}_p$ is topologically equivalent to a two dimensional annulus. (c) There exists an orbit of the state vector (X, Y) of the presented network

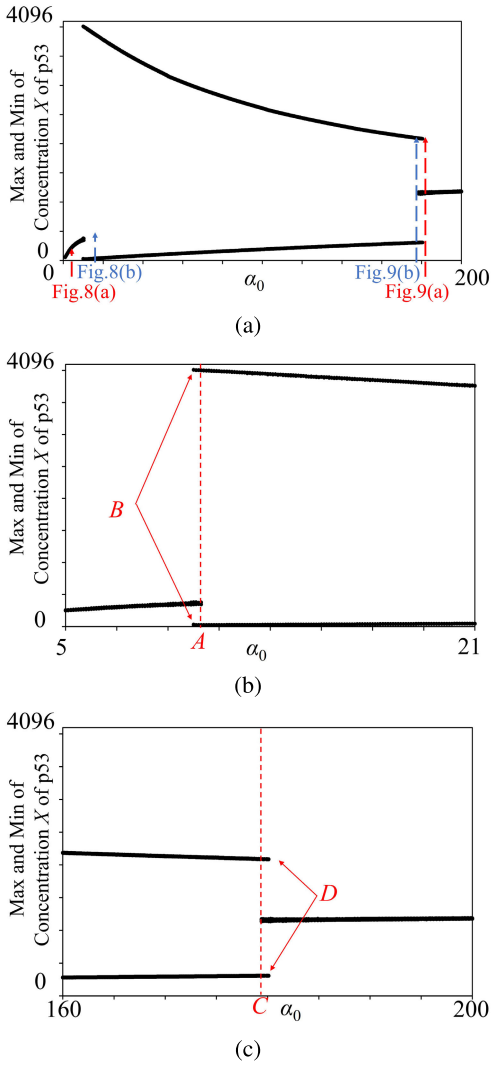

FIGURE 7. (a) Characteristics of the presented gene-protein network model obtained by numerical simulations of the dynamic equations in Eqs. (6) and (11). The horizontal axis is the parameter α_0. The vertical axis is the maximum and the minimum values of the state variable X in a steady state. (b) Enlargement of the graph in (a) near $\alpha_0 = 10$. The model exhibits a supercritical Andronov-Hopf bifurcation at A and a fold limit cycle bifurcation at B. (c) Enlargement of the graph in (a) near $\alpha_0 = 180$. The model exhibits a subcritical Andronov-Hopf bifurcation at C and a fold limit cycle bifurcation at D.

model, which ever stays in the subset $\boldsymbol{O}_p$ in a steady state. In this case, the subset $\boldsymbol{O}_p$ is referred to as a *periodic orbital set*.

The orbit of the state vector (X, Y) in Fig. 6(a) ever stays in a periodic orbital set $\boldsymbol{O}_p$ (not shown since it is almost identical with the figure of the orbit), which corresponds to the stable periodic orbit of the ODE gene-protein network model in Fig. 2(a). Next, the following definition for the phenomenon observed in Fig. 6(c) is given.

Definition 2 (Stable Equilibrium Set): Suppose there exists an orbit of the state vector (X, Y) of the presented network model starting from a subset $\boldsymbol{E} = \{(X, Y)|X = X^*_{eq}, X^*_{eq+1}, \cdots X^*_{eq+p}, Y = Y^*_{eq}, Y^*_{eq+1}, \cdots Y^*_{eq+q}\} \subset \boldsymbol{S}$ of the state space $\boldsymbol{S}$, which ever stays in the subset $\boldsymbol{E}$, where p and q are small non-negative integers. In this case, the subset $\boldsymbol{E}$ is said to be a stable equilibrium set.

The orbit of the state vector (X, Y) in Fig. 6(c) ever stays in a stable equilibrium set $\boldsymbol{E}$ (not shown since it is almost identical with the figure of the orbit), which corresponds to the stable equilibrium point of the ODE gene-protein network model in Fig. 2(c). Note that, in the case of Figs. 6(b1) and (b2), the presented model exhibits the co-existence of a periodic orbital set $\boldsymbol{O}_p$ in (b1) and a stable equilibrium set $\boldsymbol{E}$ in (b2), where the presented model exhibits one of them depending on the initial condition. In addition, this coexistence phenomenon corresponds to the co-existence phenomenon of the ODE gene-protein network model in Figs. 2(b1) and 2(b2). Fig. 7 depicts characteristics of the state variable X for the parameter α_0. It can be confirmed that the presented model exhibits the following nonlinear phenomena.

A. SUBCRITICAL Andronov-Hopf BIFURCATION

At the point A in Fig. 7(b), the stable equilibrium set $\boldsymbol{E}$ (which inactivates the DNA damage repair function) changes to the periodic orbital set $\boldsymbol{O}_p$ (which activates the DNA damage repair function) as the reproduction rate α_0 of p53 increases. This change of phenomena is qualitatively equivalent to the subcritical Andronov-Hopf bifurcation of the ODE gene-protein network model observed at the point A in Fig. 3(b). Note that the presented model has co-existing stable equilibrium set $\boldsymbol{E}$ and periodic orbital set $\boldsymbol{O}_p$ between the points A and B in Fig. 7(b), where this co-existing phenomenon is qualitatively equivalent to that of the ODE model observed in Fig. 3(b).

B. SUBCRITICAL Andronov-Hopf BIFURCATION (OPPOSITE DIRECTION)

At the point C in Fig. 7(c), the stable equilibrium set $\boldsymbol{E}$ changes to the periodic orbital set $\boldsymbol{O}_p$ as the reproduction rate α_0 of p53 decreases. This change of phenomena is qualitatively equivalent to the subcritical Andronov-Hopf bifurcation of the ODE gene-protein network model observed at the point C in Fig. 3(c). Note that the presented model has co-existing stable equilibrium set $\boldsymbol{E}$ and periodic orbital set $\boldsymbol{O}_p$ between the points C and D in Fig. 7(c), where this co-existing phenomenon is qualitatively equivalent to that of the ODE model observed in Fig. 3(c).

C. FOLD LIMIT CYCLE BIFURCATION

At the point B in Fig. 7(b), the periodic orbital set $\boldsymbol{O}_p$ disappears as the reproduction rate α_0 of p53 decreases. This change of phenomena is qualitatively equivalent to the fold limit cycle bifurcation of the ODE gene-protein network model observed at the point B in Fig. 3(b). At the point D in Fig. 7(c), the periodic orbital set $\boldsymbol{O}_p$ disappears as the reproduction rate α_0 of p53 increases. This change of phenomena is qualitatively equivalent to the fold limit cycle bifurcation of the ODE gene-protein network model observed at the point D in Fig. 3(c).

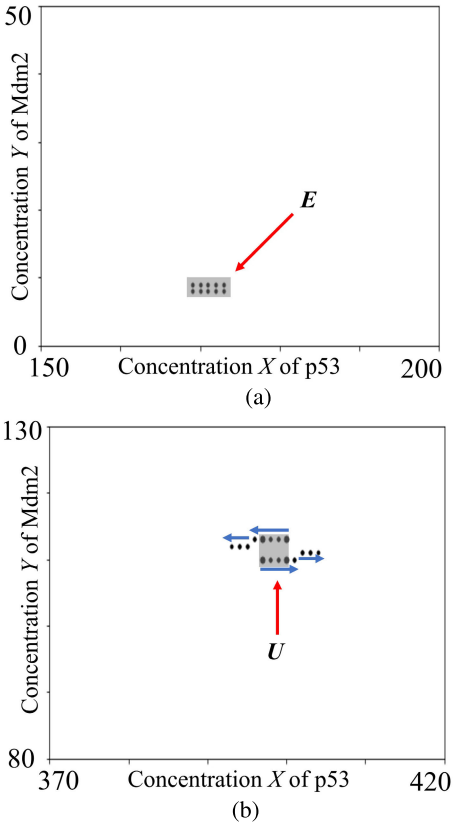

FIGURE 8. (a) Example of equilibrium set. The stable equilibrium set E is obtained by Proposition 1 theoretically. $\alpha_0 = 3$. There exists an orbit of the state vector (X, Y) that ever stays in the stable equilibrium set E. (b) Counterexample of equilibrium set. The set U does not satisfy Proposition 1. $\alpha_0 = 13$. An orbit of the state vector (X, Y) that escapes from the subset U may exist.

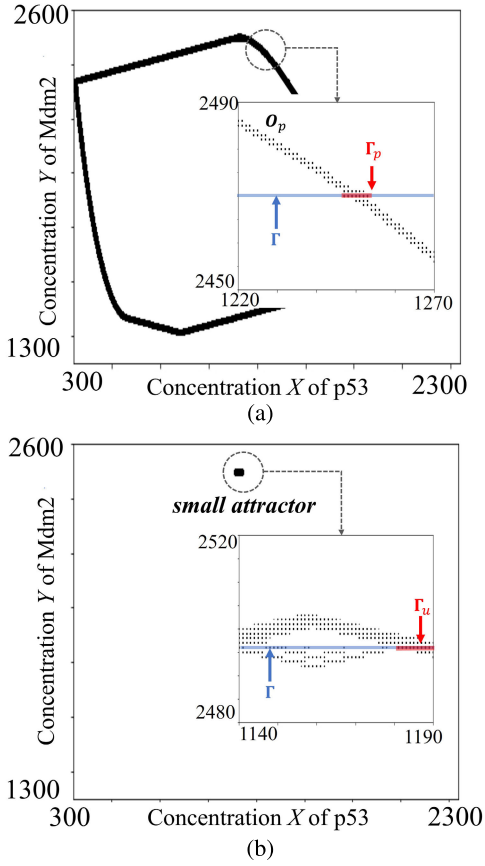

FIGURE 9. (a) Example of stable periodic set. The stable periodic set Γ_P is obtained by Proposition 2 theoretically, and corresponding periodic orbital set O_P exists. $\alpha_0 = 180$. (b) Counterexample of stable periodic set. The set Γ_u does not satisfy Proposition 2. $\alpha_0 = 179.6$. In this figure, the orbit of the state vector (X, Y) forms a small attractor, which is not a periodic orbital set.

Now we are ready to provide a sufficient condition for the existence of the stable equilibrium set $\boldsymbol{E}$ as follows.

Proposition 1: Consider a subset $\boldsymbol{E} = \{(X, Y)|X = X_{eq}, X_{eq+1}, \cdots X_{eq+p}, Y = Y_{eq}, Y_{eq+1}, \cdots Y_{eq+q}\} \subset \boldsymbol{S}$ of the state space $\boldsymbol{S}$. Suppose the initial state of the state vector (X, Y) exists in the subset $\boldsymbol{E}$ when $t = 0$. If the state vector (X, Y) stays in the subset $\boldsymbol{E}$ when $t = T$ for all initial conditions of $P \in \boldsymbol{Z}_M$, $Q \in \boldsymbol{Z}_M$, $\Phi_X \in [0, T_X)$, and $\Phi_Y \in [0, T_Y)$, then the subset $\boldsymbol{E}$ is a stable equilibrium set.

Proof: The switch signals S_X and S_Y can be generated by phase oscillators as follows.

$$
\begin{aligned}
S_X(t) &= \begin{cases} 0, & \text{if } \theta^X(t) < T_X(T_X - W_X), \\ 1, & \text{if } \theta^X(t) \geq T_X(T_X - W_X), \end{cases} \\
\theta^X(t) &= \Theta_X(t) \pmod{T_X^2}, \\
\frac{d\Theta_X(t)}{dt} &= T_X, \quad \Theta_X(0) = \Phi_X, \\
S_Y(t) &= \begin{cases} 0, & \text{if } \theta^Y(t) < T_Y(T_Y - W_Y), \\ 1, & \text{if } \theta^Y(t) \geq T_Y(T_Y - W_Y), \end{cases} \\
\theta^Y(t) &= \Theta_Y(t) \pmod{T_Y^2}, \\
\frac{d\Theta_Y(t)}{dt} &= T_Y, \quad \Theta_Y(0) = \Phi_Y. \qquad (12)
\end{aligned}
$$

Since the generators of the switch signals S_X and S_Y in Eq. (12) are deterministic, the initial phases $\theta^X(0)$ and $\theta^Y(0)$ at $t = 0$ uniquely determine the phases $\theta^X(T)$ and $\theta^Y(T)$ at $t = T$, where recall that T is the period of the clock $C(t)$. Therefore, there exist the following unique maps.

$$
\begin{aligned}
\theta^X(T) &= \mathcal{G}_{\theta^X}(\theta^X(0)), \mathcal{G}_{\theta^X} : [0, T_X^2) \to [0, T_X^2), \\
\theta^Y(T) &= \mathcal{G}_{\theta^Y}(\theta^Y(0)), \mathcal{G}_{\theta^Y} : [0, T_Y^2) \to [0, T_Y^2). \qquad (13)
\end{aligned}
$$

The time evolution of the discrete states X and Y in Eq. (6) are also deterministic, and thus the initial states $(X(0), Y(0), P(0), Q(0), \theta^X(0), \theta^Y(0))$ uniquely determine the discrete states $X(T)$ and $Y(T)$. Therefore, there exist the following unique maps.

$$
\begin{aligned}
X(T) &= \mathcal{G}_X(X(0), Y(0), P(0), \theta^X(0)), \\
Y(T) &= \mathcal{G}_Y(X(0), Y(0), Q(0), \theta^Y(0)). \qquad (14)
\end{aligned}
$$

Similarly, there exist the following unique maps.

$$
\begin{aligned}
P(T) &= \mathcal{G}_P(X(0), Y(0), P(0), \theta^X(0)), \\
Q(T) &= \mathcal{G}_Q(X(0), Y(0), Q(0), \theta^Y(0)). \qquad (15)
\end{aligned}
$$

Hence the following six-dimensional iterative map can be uniquely determined.

$$\begin{aligned} \boldsymbol{X}((n+1)T) &= \mathcal{G}(\boldsymbol{X}(nT)), \\ \boldsymbol{X}(t) &= (X(t), Y(t), P(t), Q(t), \theta^X(t), \theta^Y(t)), \\ \mathcal{G} : \boldsymbol{Z} \to \boldsymbol{Z} &= \boldsymbol{Z}_N^2 \times \boldsymbol{Z}_M^2 \times [0, T_X^2) \times [0, T_Y^2). \end{aligned} \tag{16}$$

From the conditions of the subset $\boldsymbol{E}$ in Proposition 1, we have

$$\begin{aligned} &(X(T), Y(T)) = (\mathcal{G}_X(\boldsymbol{X}(0)), \mathcal{G}_Y(\boldsymbol{X}(0))) \subseteq \boldsymbol{E} \\ &\text{for all } (X(0), Y(0)) \in \boldsymbol{E} \text{ and for all} \\ &(P(0), Q(0), \theta^X(0), \theta^Y(0)) \in \boldsymbol{Z}_M^2 \times [0, T_X^2) \times [0, T_Y^2). \end{aligned} \tag{17}$$

Then, from the mathematical induction, we have

$$(X(nT), Y(nT)) \subseteq \boldsymbol{E} \quad \text{for all } (X(0), Y(0)) \in \boldsymbol{E}. \tag{18}$$

Since the situation in Eq. (18) is identical with the definition of the equilibrium set $\boldsymbol{E}$ in Definition 2, Proposition 1 is proven, where the lengths p and q of $\boldsymbol{E}$ are assumed to be small. Q.E.D.

D. EXAMPLE AND COUNTEREXAMPLE 1

For example, the subset $\boldsymbol{E}$ in Fig. 8(a) satisfies Proposition 1 and thus it can be theoretically guaranteed that the subset $\boldsymbol{E}$ is a stable equilibrium set. Then Proposition 1 guarantees that there exists an orbit of the state vector (X, Y) of the presented gene-protein network model that ever stays in the stable equilibrium set $\boldsymbol{E}$ as shown in Fig. 8(a). On the contrary, the subset $\boldsymbol{U}$ in Fig. 8(b) is a counterexample, i.e., the subset $\boldsymbol{U}$ does not satisfy Proposition 1 and thus it cannot be guaranteed that the subset $\boldsymbol{U}$ is a stable equilibrium set. In this case, an orbit of the state vector (X, Y) that escapes from the subset $\boldsymbol{U}$ may exist as shown in Fig. 8(b).

Next, we give the following definition related to the periodic orbital set $\boldsymbol{O}_p$ (see also Fig. 9).

Definition 3: Suppose there exists a subset $\boldsymbol{\Gamma} = \{(X, Y) | X \in \boldsymbol{Z}_N, Y = Y_\Gamma\} \subset \boldsymbol{S}$ of the state space $\boldsymbol{S}$, which satisfies the following two conditions. (i) There exists a subset $\boldsymbol{\Gamma}_p = \{(X, Y) | X \in \{X_p, X_p + 1, \cdots, X_p + r\}, Y = Y_\Gamma\} \subset \boldsymbol{\Gamma}$, where r is a small non-negative integer. (ii) The trajectories of (X, Y) starting from the subset $\boldsymbol{\Gamma}_p$ ever repeats the following itinerancy: escape from $\boldsymbol{\Gamma}_p$ to the subset $\{(X, Y) | X \in \boldsymbol{Z}_N, Y \geq Y_\Gamma\}$; keeps $Y \geq Y_\Gamma$ and returns to the subset $\boldsymbol{\Gamma} \setminus \boldsymbol{\Gamma}_p$; escape from the subset $\boldsymbol{\Gamma} \setminus \boldsymbol{\Gamma}_p$ to the subset $\{(X, Y) | X \in \boldsymbol{Z}_N, Y \leq Y_\Gamma\}$; and keeps $Y \leq Y_\Gamma$ and returns to the subset $\boldsymbol{\Gamma}_p$. In this case, the subset $\boldsymbol{\Gamma}_p$ is said to be a stable periodic set.

Fig. 9 shows an example of the stable periodic set $\boldsymbol{\Gamma}_p$. Then we give the following sufficient condition for the existence of the stable periodic set $\boldsymbol{\Gamma}_p$.

Proposition 2: Consider subsets $\boldsymbol{\Gamma} = \{(X, Y) | X \in \boldsymbol{Z}_N, Y = Y_\Gamma\} \subset \boldsymbol{S}$ and $\boldsymbol{\Gamma}_p = \{(X, Y) | X \in \{X_p, X_p + 1, \cdots, X_p + r\}, Y = Y_\Gamma\} \subset \boldsymbol{\Gamma}$. If any trajectory of (X, Y) starting from the subset $\boldsymbol{\Gamma}_p$ travels the itinerancy defined in Definition 3 and returns to the subset $\boldsymbol{\Gamma}_p$, then the subset $\boldsymbol{\Gamma}_p$ is a stable periodic set. In this case, the trajectories of (X, Y) starting from the stable periodic set $\boldsymbol{\Gamma}_p$ for all initial conditions of $P \in \boldsymbol{Z}_M$, $Q \in \boldsymbol{Z}_M$, $\Phi_X \in [0, T_X)$, and $\Phi_Y \in [0, T_Y)$ form a periodic orbital set $\boldsymbol{O}_p$.

Proof: From Eq. (16), the trajectory of the state vector $\boldsymbol{X}(nT)$ $(n = 1, 2, \cdots)$ can be uniquely determined by the initial state $\boldsymbol{X}(0)$. Therefore, from the conditions in Proposition 2, we can find the minimum integer $k_1 \geq 1$ such that

$$\begin{aligned} &(X(k_1 T), Y(k_1 T)) \subseteq \boldsymbol{\Gamma}_p \\ &\text{for each } (X(0), Y(0)) \in \boldsymbol{\Gamma}_p \text{ and for each} \\ &(P(0), Q(0), \theta^X(0), \theta^Y(0)) \in \boldsymbol{Z}_M^2 \times [0, T_X^2) \times [0, T_Y^2). \end{aligned} \tag{19}$$

Then, from the mathematical induction, we can find the minimum integers k_n $(n = 1, 2, 3, \cdots)$ such that

$$\begin{aligned} &(X(k_n T), Y(k_n T)) \subseteq \boldsymbol{\Gamma}_p \\ &\text{for each } (X(0), Y(0)) \in \boldsymbol{\Gamma}_p \text{ and for each} \\ &(P(0), Q(0), \theta^X(0), \theta^Y(0)) \in \boldsymbol{Z}_M^2 \times [0, T_X^2) \times [0, T_Y^2), \end{aligned} \tag{20}$$

where the trajectory of the state vector (X, Y) starting from the initial state $(X(0), Y(0))$ repeats the itinerancy in Proposition 2. Since n can be plus infinity, it is guaranteed that the trajectory of the state vector (X, Y) ever repeats the itinerancy in Proposition 2. Hence the subset $\boldsymbol{\Gamma}_p$ satisfies the conditions in Definition 3 and thus it is a stable periodic set. Eq. (6) guarantees that any state vector (X, Y) starting from $\boldsymbol{\Gamma}_p$ forms a set of connected points. Since the state vector (X, Y) starting from $\boldsymbol{\Gamma}_p$ ever repeats the itinerancy in Proposition 2, it forms a subset that is topologically equivalent to a two dimensional annulus. Hence the trajectory of the state vector (X, Y) starting from the initial state $\boldsymbol{\Gamma}_p$ forms a periodic orbital set. Q.E.D.

E. EXAMPLE AND COUNTEREXAMPLE 2

For example, the subset $\boldsymbol{\Gamma}_p$ in Fig. 9(a) satisfies Proposition 2 and thus it can be theoretically guaranteed that the subset $\boldsymbol{\Gamma}_p$ is a stable periodic set. Then Proposition 2 guarantees that there exists an orbit of the state vector (X, Y) of the presented gene-protein network model that ever returns back in the stable periodic set $\boldsymbol{\Gamma}_p$. In this case, a periodic orbital set $\boldsymbol{O}_p$ exists as shown in Fig. 9(a). On the contrary, the subset $\boldsymbol{\Gamma}_u$ in Fig. 9(b) is a counterexample, i.e., the subset $\boldsymbol{\Gamma}_u$ does not satisfy Proposition 2 and thus it cannot be guaranteed that the subset $\boldsymbol{\Gamma}_u$ is a stable periodic set. In this case, an orbit of the state vector (X, Y) that does not form a periodic orbital set may exist, e.g., the orbit of the state vector (X, Y) in Fig. 9(b) forms a small attractor, which is not a periodic orbital set.

To show a theoretical advantage of the presented model, the following definitions are given.

Definition 4 (Ergodic Cellular Automaton): Let $\theta^X(n)$ and $\theta^Y(n)$ represent the phases of the switch signals $S_X(t)$ and $S_Y(t)$ sampled at the n-th pulsed moment of the clock $C(t)$, respectively. Suppose the clock $C(t)$ and the switch signals S_X

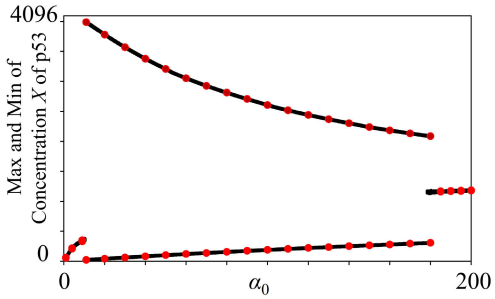

FIGURE 10. Characteristics of the ergodic cellular automaton gene-protein network model. The black graphs are obtained numerically. The red points are obtained theoretically by Propositions 1 and 2. $(\alpha_1, \alpha_2, \alpha_3, k_1, k_2, \gamma_1, \gamma_2, \gamma_3)$ are as in Fig. 2. $(N, M, T_C, T_X, \Phi_X, W_X, T_Y, \Phi_Y, W_Y, \Omega_X, \Omega_Y) = (4096, 2, 3\sqrt{5}\,10^{-6}, 3\sqrt{5}\,10^{-6}, 0, 3\sqrt{5}\,10^{-6}, 5\sqrt{48}10^{-6}, 0, 3\sqrt{5}\,10^{-6}, 64, 64)$.

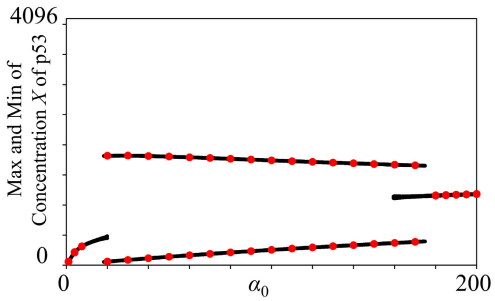

FIGURE 11. Characteristics of the regular cellular automaton gene-protein network model. The black graphs are obtained numerically. The red points are obtained theoretically by Propositions 1 and 2 and their symmetric ones. $(\alpha_1, \alpha_2, \alpha_3, k_1, k_2, \gamma_1, \gamma_2, \gamma_3)$ are as in Fig. 2. $(N, M, T_C, T_X, \Phi_X, W_X, T_Y, \Phi_Y, W_Y, \Omega_X, \Omega_Y) = (4096, 2, 5 \cdot 10^{-6}, 5 \cdot 10^{-6}, 0, 5 \cdot 10^{-6}, 5 \cdot 10^{-6}, 0, 5 \cdot 10^{-6}, 64, 64)$.

and S_Y are supplied by generators, which are not connected physically. In this case, the sampled phases $\theta^X(n)$ and $\theta^Y(n)$ become non-periodic and ergodic. In addition, the variables X, Y, P, and Q mostly transit locally like a cellular automaton. Hence the proposed model is said to be an ergodic cellular automaton gene-protein network model.

Definition 5 (Regular Cellular Automaton): Suppose the generators of the clock $C(t)$ and the switch signals S_X and S_Y are connected physically, and $C(t)$, $S_X(t)$, and $S_Y(t)$ are phase-locked. In this case, the sampled phases $\theta^X(n)$ and $\theta^Y(n)$ become constant or periodic. Since the typical case $T_C = T_X = T_Y$ corresponds to a standard non-ergodic cellular automaton, the model is said to be a regular cellular automaton gene-protein network model.

Then the following remarks are given.

Remark 3 (Theoretical Advantage of Ergodic CA):

- Fig. 10 shows the theoretical characteristics of the stable equilibrium set $\boldsymbol{E}$ and the periodic orbital set $\boldsymbol{O}_p$ of the ergodic cellular automaton gene-protein network model obtained by Propositions 1 and 2. By comparing Fig. 10 and Fig. 3, it can be concluded that the ergodic cellular automaton gene-protein network model can reproduce the characteristics of the ODE gene-protein network model.
- Fig. 11 shows the theoretical characteristics of the stable equilibrium set $\boldsymbol{E}$ and the periodic orbital set $\boldsymbol{O}_p$ of a regular cellular automaton gene-protein network model obtained by Propositions 1 and 2. By comparing Fig. 11 and Fig. 3, it can be concluded that the regular cellular automaton gene-protein network model cannot reproduce the characteristics of the ODE gene-protein network model.
- Therefore, Propositions 1 and 2 theoretically reveal that the ergodic cellular automaton is better suited to build a gene network simulator compared to the regular cellular automaton.

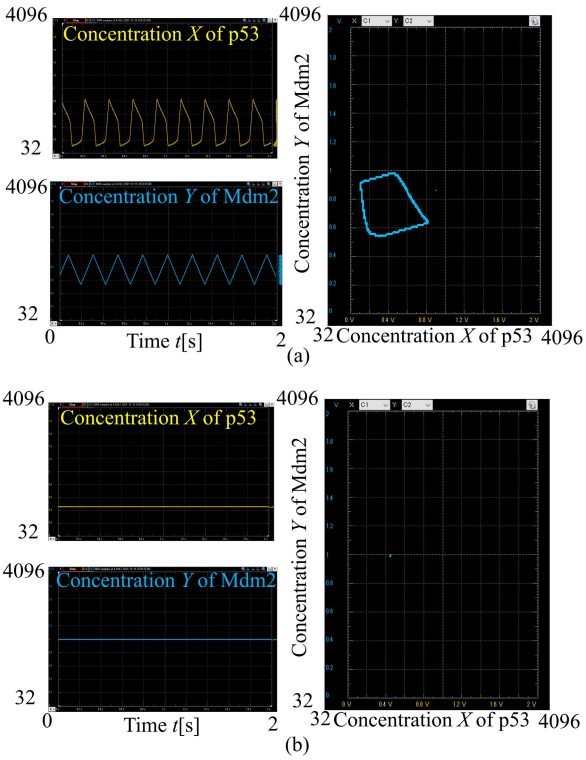

FIGURE 12. Oscilloscope snapshots showing typical time waveforms and corresponding phase plane trajectories of the ergodic cellular automaton gene-protein network model implemented by the FPGA. The parameter values are as in Fig. 6. (a) Oscillating orbit corresponding to the periodic orbital set O_p in Fig. 6(a). $\alpha_0 = 175$. (b) Resting orbit corresponding to the stable equilibrium set E in Fig. 6(c). $\alpha_0 = 185$.

V. IMPLEMENTATION AND COMPARISON

A. IMPLEMENTATION

The dynamics of the presented ergodic cellular automaton gene-protein network model described in Eqs. (2), (3), (8), (9), (6) and (11) were handwritten in a register transfer level Verilog-HDL code, where a pseudo HDL code is given in Appendix A. The handwritten Verilog-HDL code was compiled by Xilinx's design suite Vivado 2021.1 and the generated bitstream file was used to implement Xilinx's field programmable gate array (FPGA) device XC7A200T-1SBG484C consisting of 33,650 logic slices, where each logic slice includes four 6-input LUTs and eight flip-flops. The resulting hardware can be regarded as a customized

TABLE 1. Comparisons with other hardware implementation methods. ∗The typical values and the average values of the features of the hardware are obtained for the parameter value $\alpha_0 = 100$ and the parameter values $\alpha_0 = 20, 40, 60, 80, 100, 120, 140, 160$, respectively.

Mathematical model	Ergodic cellular automaton		Regular cellular automaton		Numerical integration		Numerical integration	
Circuit architecture	Ergodic sequential logic		Synchronous sequential logic		Customized DSP implemented on FPGA		Customized CPU implemented on FPGA	
Design method	Handwritten RTL HDL code		Handwritten RTL HDL code		Handwritten RTL HDL code		Soft CPU (IP core), C language	
Design tool	Xilinx's design suite Vitis 2021.1							
Implementation Device	Xilinx's FPGA XC7A200T-1SBG484C							
Clock frequency [MHz]	0.1		0.1		0.1		100	
Resolution of state space	$M = 2$ (1-bit unsigned integer), $N = 4096$ (12-bit unsigned integer)		$M = 2$ (1-bit unsigned integer), $N = 4096$ (12-bit unsigned integer)		56-bit fixed point number		64-bit floating point number	
	Typical*	Average*	Typical*	Average*	Typical*	Average*	Typical*	Average*
Number of logic slices	338	341	343	336	11929	11972	578	578
Number of look-up tables	1148	1162	1147	1162	41539	41530	1444	1444
Number of flip-flops	172	172	172	172	267	267	1456	1456
On-chip Power [mW]	20	20	23	23	1732	1722	132	132
Energy [mJ] used to simulate one period of oscillation	5.58	5.84	1.69	1.69	7.46	8.67	717	717
Reproduction of bifurcations in Fig. 3	Possible as in Fig. 10		Not possible as in Fig. 11		Possible		Possible	
Remark	Model of choice		Bifurcations cannot be simulated		Large circuit		High energy	

ergodic sequential logic that is especially designed to operate Eqs. (6) and (11). Fig. 12 shows typical waveforms of the implemented ergodic cellular automaton gene-protein network model, which correspond to those in Fig. 6 (a) and (c).

B. COMPARISONS

For comparison, the regular cellular automaton gene-protein network model (which can be regarded as a synchronous sequential logic gene-protein network model) and a forward Euler formula of the ODE gene-protein network model (which can be regarded as a customized digital signal processor (DSP) gene-protein network model) were implemented in the same manner, i.e., these models were handwritten in register transfer level Verilog-HDL codes, the codes were compiled by the same design software, and the generated bitstream files were used to implement the same FPGA device. In addition, a CPU is implemented in the same FPGA device by using Xilinx's soft microprocessor Microblaze, where the forward Euler formula of the ODE gene-protein network model was handwritten in a C programming language code, the code was compiled by Xilinx's software platform Vitis 2021.1, and the generated binary file was used to operate the CPU. Note that the CPU is especially customized to execute the forward Euler formula of the ODE gene-protein network model. Table 1 summarizes comparison results under the following conditions and constraints.

C1 The bit lengths of the discrete variables (i.e., resolution of the state space) of the cellular automaton models and the DSP model were shortened as short as possible under the condition that the models operated properly (see also Appendix B). The bit length of the CPU was set to 64-bit based on the default feature of the soft microprocessor.

C2 The value of the parameter α_0 of each model was set to 20, 40, 60, $\cdots$, and 160, which lead to multiple different oscillations of the state variable X.

C3 For comparison, the energy used to simulate one period of oscillation of X was derived for each model, where the energy was calculated as the product of the oscillation period and the on-chip dynamic power.

It can be confirmed in Table 1 that the presented ergodic cellular automaton model is the model of choice since (a) it can predict the parameter values that cause the bifurcations of the ODE gene-protein network model while the regular cellular automaton model cannot, and (b) it is more hardware-efficient (i.e., consumes much fewer circuit elements and lower energy) compared to the DPS model and the CPU mode. The fundamental reason why the presented cellular automaton model consumes fewer circuit elements (and thus consumes lower energy) compared to the DPS model and the CPU model is that the resolutions of the discrete functions $(\mathcal{F}_X, \mathcal{F}_Y)$ in Eq. (8) of the cellular automaton model are much lower and are implemented by LUTs while the resolutions of the nonlinear functions in Eq. (1) of the DSP model and the CPU model must be much higher to realize proper calculations of the numerical integration and are implemented by multipliers.

Algorithm 1 Pseudo hdl code of the presented model

```
/* Definitions of discrete state variables X and Y in Eq. (2) and discrete auxiliary variables P and Q in Eq. (3) */
reg signed [15:0] X;          reg signed [15:0] Y;          reg signed [15:0] P;          reg signed [15:0] Q
reg signed [15:0] X_new;  reg signed [15:0] Y_new;  reg signed [15:0] P_new;  reg signed [15:0] Q_new;
/* Implementations of the functions F_X and F_Y in Eq. (9) as LUTs */
/* The values denoted by ??? are pre-calculated using Eq. (9)          */
reg signed [15:0] LUT_X_BORDER[4095:0];      reg signed [15:0] LUT_Y_BORDER[4095:0];
initial LUT_X_BORDER[0] = ???;  initial LUT_X_BORDER[1] = ???;  ···;  initial LUT_X_BORDER[4095] = ???;
initial LUT_Y_BORDER[0] = ???;  initial LUT_Y_BORDER[1] = ???;  ···;  initial LUT_Y_BORDER[4095] = ???;
/* Definitions of the return values of the discrete funtions F_X and F_Y in Eq. (8) */
reg signed [1:0] FX;  reg signed [1:0] FY;
/* Transitions of the discrete variables (X, Y, P, Q) in Eqs. (6) and (11) triggered by the clock C. */
/* Reset is omitted for simplicity.                                                                  */
always@(posedge C) begin
    if (SX == 1) begin
    if (LUT_X_BORDER[X] > Y) FX = 1;  else FX = −1;
        if ((P < FX && FX > 0) || (P < −FX && FX < 0)) P_new = P + 1;
        else begin
            P_new = 0;
            if (X < 4095 && FX >= 0) X_new = X + 1;  else if (X > 0 && FX < 0) X_new = X −1;
        end
    end
    if (SY == 1) begin
        if (LUT_Y_BORDER[X] > Y) FY = 1;  else FY = −1;
        if ((Q < FY && FY > 0) || (Q < −FY && FY < 0)) Q_new = Q + 1;
        else begin
            Q_new = 0;
            if (Y < 4095 && FY >= 0) Y_new = Y + 1;  else if (Y > 0 && FY < 0) Y_new = Y −1;
        end
    end
    X = X_new;  P = P_new;  Y = Y_new;  Q = Q_new;
end
```

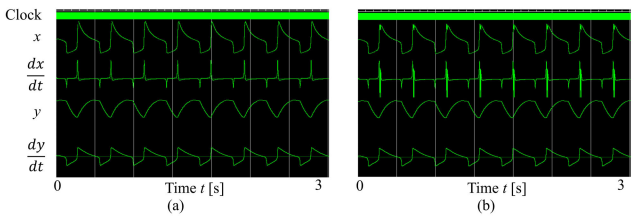

FIGURE 13. Numerical simulations showing typical time waveforms of the DSP gene-protein network model in Subsection III-B. (a) The bit length of the state variables is 56-bit. The model operates properly. (b) The bit length of the state variables is 55-bit. The model does not operate properly (see the unexpected fast oscillations at the peak of the state variable x).

VI. CONCLUSION

The theoretical analysis methods proposed in this study revealed that the presented ergodic cellular automaton gene-protein network model is better suited to predict the parameter values that cause the bifurcations of the ODE gene-protein network model compared to the regular cellular automaton model. In addition, the FPGA implementations and comparisons revealed that the presented model is much more hardware-efficient (e.g., consumes much fewer circuit elements and much lower power) compared to the standard numerical integration model of the gene-protein network. Hence the results of this paper will provide fundamental knowledge about designing a hardware-efficient application specific integrated circuit for the genome simulation. To realize such a future hardware-based genome simulator, the following problems should be solved. (a) development of design methods of the ergodic cellular automaton model that can reproduce a wide variety of bifurcations precisely, (b) development of a systematic design method of ergodic cellular automaton models of large-scale gene-protein networks, (c) development of theoretical analysis methods of such large-scale ergodic cellular automaton networks, (d) development of a systematic implementation method of such large-scale ergodic cellular automaton networks, and (e) clarification of relationship between the ergodic cellular automaton and other similar dynamical systems such as the fuzzy logic network [21].

APPENDIX A

See Algorithm 1.

APPENDIX B (BIT LENGTH OF THE DSP GENE-PROTEIN NETWORK MODEL)

As explained in the condition C1 of the comparison in Subsection III-B, the bit length of the discrete variables of the DSP gene-protein network model was shortened as short as possible under the condition that the model operated properly. Base on the numerical simulations including the ones in Fig. 13, the bit-length of the DSP model was set to 56-bit in this study.

REFERENCES

[1] K. Rateitschak and O. Wolkenhauer, "Thresholds in transient dynamics of signal transduction pathways," *J. Theor. Biol.*, vol. 264, no. 2, pp. 334–346, May 2010.
[2] S. Schuster, D. A. Fell, and T. Dandekar, "A general definition of metabolic pathways useful for systematic organization and analysis of complex metabolic networks," *Nature Biotechnol.*, vol. 18, no. 3, pp. 326–332, Mar. 2000.
[3] B. Mazumder, X. Li, and S. Barik, "Translation control: A multifaceted regulator of inflammatory response," *J. Immunol.*, vol. 184, no. 7, pp. 3311–3319, Apr. 2010.
[4] J.-X. Yue and G. Liti, "SimuG: A general-purpose genome simulator," *Bioinformatics*, vol. 35, no. 21, pp. 4442–4444, Nov. 2019.
[5] F. Pappalardo, P. Zhang, M. Halling-Brown, K. Basford, A. Scalia, A. Shepherd, D. Moss, S. Motta, and V. Brusic, "Computational simulations of the immune system for personalized medicine: State of the art and challenges," *Current Pharmacogenomics Personalized Med.*, vol. 6, no. 4, pp. 260–271, Dec. 2008.
[6] B. Bansal, A. Nanda, and A. Sahoo, "Intelligent framework with controlled behavior for gene regulatory network reconstruction," *Int. J. Inf. Retr. Res.*, vol. 12, no. 1, pp. 1–17, Jan. 2022.
[7] S. Komaki, K. Takeda, and H. Torikai, "A novel ergodic discrete difference equation model of central pattern generator: Theoretical analysis and efficient implementation," *IEEE Trans. Circuits Syst. II, Exp. Briefs*, vol. 69, no. 3, pp. 1767–1771, Mar. 2022.
[8] Z. Li, P. Li, A. Krishnan, and J. D. Liu, "Large-scale dynamic gene regulatory network inference combining differential equation models with local dynamic Bayesian network analysis," *Bioinformatics*, vol. 27, no. 19, pp. 2686–2691, 2011.
[9] L. Minati, M. Frasca, N. Yoshimura, and Y. Koike, "Versatile locomotion control of a hexapod robot using a hierarchical network of nonlinear oscillator circuits," *IEEE Access*, vol. 6, pp. 8042–8065, 2018.
[10] C. Mayr, "A biological-realtime neuromorphic system in 28 nm CMOS using low-leakage switched capacitor circuits," *IEEE Trans. Biomed. Circuits Syst.*, vol. 10, no. 1, pp. 243–254, Feb. 2016.
[11] B. Zhong, S. Zhang, M. Xu, Y. Zhou, T. Fang, and W. Li, "On a CPG-based hexapod robot: AmphiHex-II with variable stiffness legs," *IEEE/ASME Trans. Mechatronics*, vol. 23, no. 2, pp. 542–551, Apr. 2018.
[12] E. I. Guerra-Hernandez, "A FPGA-based neuromorphic locomotion system for multi-legged robots," *IEEE Access*, vol. 5, pp. 8301–8312, 2017.
[13] K. Takeda and H. Torikai, "A novel hardware-efficient central pattern generator model based on asynchronous cellular automaton dynamics for controlling hexapod robot," *IEEE Access*, vol. 8, pp. 139609–139624, 2020.
[14] K. Takeda and H. Torikai, "A novel hardware-oriented recurrent network of asynchronous CA neurons for a neural integrator," *IEEE Trans. Circuits Syst. II, Exp. Briefs*, vol. 68, no. 8, pp. 2972–2976, Aug. 2021.
[15] K. Takeda and H. Torikai, "A novel asynchronous CA neuron model: Design of neuron-like nonlinear responses based on novel bifurcation theory of asynchronous sequential logic circuit," *IEEE Trans. Circuits Syst. I, Reg. Papers*, vol. 67, no. 6, pp. 1989–2001, Jun. 2020.
[16] K. Takeda and H. Torikai, "A novel hardware-efficient cochlea model based on asynchronous dynamics," *IEEE Trans. Circuits Syst. II, Exp. Briefs*, vol. 64, no. 9, pp. 1107–1111, Sep. 2017.
[17] X. Jun-Feng and J. Ya, "A mathematical model of a P53 oscillation network triggered by DNA damage," *Chin. Phys. B*, vol. 19, no. 4, Apr. 2010, Art. no. 040506.
[18] S. Haupt, M. Berger, Z. Goldberg, and Y. Haupt, "Apoptosis–the p53 network," *J. Cell Sci.*, vol. 116, no. 20, pp. 4077–4085, Oct. 2003.
[19] V. Chickarmane, A. Ray, H. M. Sauro, and A. Nadim, "A model for p53 dynamics triggered by DNA damage," *SIAM J. Appl. Dyn. Syst.*, vol. 6, no. 1, pp. 61–78, Jan. 2007.
[20] Y. A. Kuznetsov, "One-parameter bifurcation of equilibria in continuous-time dynamical system," in *Elements of Applied Bifurcation Theory*, 3rd ed. New York, NY, USA: Springer, 2004, ch. 3, pp. 77–102.
[21] M. Bucolo, L. Fortuna, and M. L. Rosa, "Complex dynamics through fuzzy chains," *IEEE Trans. Fuzzy Syst.*, vol. 12, no. 3, pp. 289–295, Jun. 2004.

SHOGO SHIRAFUJI (Student Member, IEEE) received the bachelor's degree in science and engineering from Hosei University, Tokyo, Japan, in 2021. He is currently a Graduate Student with the Graduate School of Science and Engineering, Hosei University. His current research interests include nonlinear dynamics, biomimetic engineering, and digital circuit design.

HIROYUKI TORIKAI (Member, IEEE) received the B.E., M.E., and Ph.D. degrees in electrical engineering from Hosei University, Tokyo, Japan, in 1995, 1997, and 1999, respectively. He is currently a Professor with the Faculty of Science and Engineering, Hosei University. His current research interests include nonlinear dynamics, neural networks, and discrete state dynamics.